TÜBİTAK

Turk J Elec Eng & Comp Sci, Vol.20, No.3, 2012, © TÜBİTAK
doi:10.3906/elk-1003-431

Investigating the relation between optimum guard interval and channel delay spread for a MC-CDMA system

Çetin KURNAZ, Hülya GÖKALP*
Department of Electrical and Electronics Engineering, Ondokuz Mayıs University, Samsun-TURKEY
e-mail: ckurnaz@omu.edu.tr, hgokalp@omu.edu.tr

Received: 22.03.2010

Abstract

This paper demonstrates a novel approach to determining the optimum guard interval for a multicarrier code division multiple access (MC-CDMA) system. Analytical expressions for useful and interference power are derived as a basis for comparison. From these, an expression for the signal-to-noise ratio of a detected bit is derived and used to determine the optimum guard interval for a given channel profile and system parameters. In contrast to other works, we use channel models based on actual measurements and we highlight important differences from theoretical models to support our approach. From our results, we propose an empirical rule for optimum guard intervals given prevailing channel parameters. We show that the optimum guard interval can be selected as the delay window that includes 95% and 99% multipath power for E_s/N_0 *= 10 dB and* E_s/N_0 *= 20 dB, respectively. In our case, the optimum guard interval was between 2* τ_{rms} *and 4* τ_{rms} *for* E_s/N_0 *= 10 dB and between 3* τ_{rms} *and 6.4* τ_{rms} *for* E_s/N_0 *= 20 dB.*

Key Words: *Optimum guard interval, multicarrier code division multiple access, outdoor radio channel, root-mean-square delay spread, Delay window*

1. Introduction

Wireless communication systems aim to support services with a range of data rates over limited transmission bandwidths. Multicarrier code division multiple access (MC-CDMA) is among the techniques being considered for future generations of wireless systems due to its robustness against frequency selective fading and its capability to support wireless communication in outdoor environments with diverse frequency selective propagation [1-5]. In MC-CDMA, frequency diversity is achieved by transmitting the chips of a symbol over multiple subcarriers [6]. MC-CDMA can accommodate many users within a specified band and can have computationally

*Corresponding author: Department of Electrical and Electronics Engineering, Ondokuz Mayıs University, Samsun-TURKEY

efficient transmission and reception through the use of inverse fast Fourier transform/fast Fourier transform techniques. Moreover, for downlinks where linear amplification is possible, the spectral efficiency can be increased further for mobiles with low speed by placing the subcarriers closer together in the frequency domain.

Intersymbol interference (ISI) due to time dispersion of the multipath channel deteriorates the performance of the MC-CDMA system. Approaches to reduce the effects of ISI include employing iterative interference reduction techniques [7] or using preequalization at the transmitter and postequalization at the receiver [8], but these increase the computational complexity of the system. It is possible to use equalization techniques that exploit guard interval (T_G) redundancy to reduce the computational complexity [9], or to simply use a guard interval with a cyclic prefix. The cyclic prefix used in the guard interval converts the linear convolution of the transmitted symbol with the channel impulse response into circular convolution and simplifies the channel equalization. To avoid ISI without increasing computational complexity, a guard interval that is longer than the significant part of the channel impulse response may be used.

In previous work on guard intervals, optimization was typically achieved using 2 hypothetical models for the channel: either an exponentially decaying profile with uniformly distributed multipath arrivals or a 2-ray equal-power profile [10,11]. However, real channels differ in their properties and multipath components typically arrive in clusters with different decay rates. The 2-ray equal-power profile can represent the worst-case frequency selectivity [12,13] and is widely used in the optimization of the number of subcarriers for multicarrier systems. In the case of such a profile, 2 options for the guard interval exist: $0 < T_G < 2\tau_{rms}$ (a T_G value slightly greater than 0 μs will suffice), where the second arriving ray contributes to ISI; and $T_G > 2\tau_{rms}$, where no multipath components exceed the guard interval and there is hence no ISI. In both cases, the ratio of T_G/τ_{rms} may be fixed and therefore may not be suitable for optimization.

Alternatively, some multiples of the root-mean-square (rms) delay spread of the channel, using widely published rms delay spread (τ_{rms}) data, are used as an appropriate guard interval ($\mathrm{T}_{G,opt}$). A further method is to take a fraction of the symbol period (T_s). For example, in [6,14], the guard interval was chosen to be 4 times the τ_{rms}, in [11,15] to be 20% of the symbol period, and in [16] to be 25% of the symbol period.

In contrast, this paper uses channel models based on actual measurements to optimize the guard interval for MC-CDMA systems. The purpose of the work is to derive an analytical expression that can be used to optimize the guard interval for a given channel profile. For this, analytical expressions for useful power, interference power, and the signal-to-noise ratio (SNR) at the detector output of the MC-CDMA system are derived. Using these, the optimum guard interval, $\mathrm{T}_{G,opt}$, is determined as the guard interval with a maximum SNR. The paper further investigates the relationship between the optimum guard interval and prevailing channel parameters to determine an empirical rule. The relation of the optimum guard interval to the rms delay spread, symbol period, and width of delay window is investigated. The paper considers the differences in results between theoretical models and models based on actual measurements.

2. MC-CDMA system model

The MC-CDMA system model comprises 3 main functional blocks: a transmitter, radio channel, and receiver. The output of the transmitter is fed into the radio channel block (Figure 1). In the radio channel, the signal undergoes frequency selective fading and is corrupted with additive white Gaussian noise (AWGN). The output of the radio channel is then fed into the receiver block.

2.1. Transmitter

At the transmitter, the input data sequence is segmented into blocks of L bits. Each L-bit block is passed through serial-to-parallel (S/P) conversion, i.e. each transmitted symbol contains L data bits. Each S/P converter output is spread using a spreading code of length N (Figure 1). All of the chips for a data segment (N × L chips) are modulated with binary phase-shift keying in the base band by the inverse discrete Fourier transform (IDFT) block. The NL chips are converted back into a serial sequence. The last υ chips corresponding to the guard interval are copied and used as the cyclic prefix. After adding the cyclic prefix, the data are fed to the radio channel.

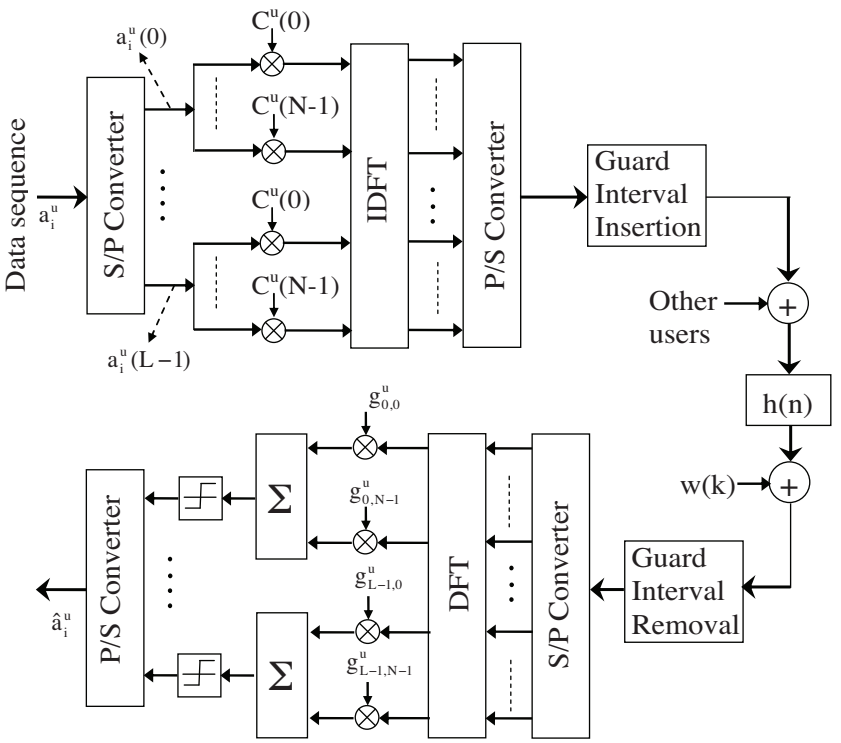

Figure 1. MC-CDMA transmitter, radio channel, and receiver.

At the transmitter, the φth output of the IDFT block for the uth user can be given as:

$$s_{i,\phi}^{u} = \sqrt{\frac{E_s}{NL+\upsilon}} \sum_{\ell=0}^{L-1} \sum_{n=0}^{N-1} a_i^u(\ell)\, C^u(n)\, e^{j2\pi\phi\frac{(N\ell+n)}{NL}}, \quad \phi = -\upsilon, ..., NL-1, \tag{1}$$

where N is the length of the spreading sequence, L is the number of bits involved in the S/P conversion, E_s is the energy per symbol, $a_i^u(\ell)$ is the ℓ^{th} output of the S/P converter for the ith information symbol of the uth user, $C^u(n)$ is the nth chip of the spreading code of the uth user, υ is the number of chips within the guard interval (T_G), and $NL + \upsilon$ is the number of chips within the symbol period (T_s).

2.2. Receiver

The received signal is the sum of the MC-CDMA signals transmitted by all active users in the cell. After removal of the cyclic prefix, the received signal can be written in discrete form as:

$$r(k) = \sum_{u=0}^{U-1} \sum_{i=-\infty}^{+\infty} \sum_{\phi=-\upsilon}^{NL-1} s_{i,\phi}^{u}\, h\left[(k-\phi) - i\left(NL+\upsilon\right)\right] + w(k)\,, \tag{2}$$

where U is the total users, w(k) is the AWGN for the kth output, and h(n) is the discrete form of the channel impulse response. For h(n), we can write:

$$h(n) = 0 \begin{cases} n < 0 \\ n \geq NL + \upsilon \end{cases} . \tag{3}$$

The received signal is segmented into subsequences of $NL+\upsilon$ chips and each sequence is S/P-converted. First, the cyclic prefix is removed, and then the signal is demodulated via the discrete Fourier transform (DFT). The output of the demodulator can be written as:

$$Z_{\ell',n'} = \sqrt{\frac{1}{NL}} \sum_{k=0}^{NL-1} r\left(k\right) e^{-j2\pi k \frac{(N\ell'+n')}{NL}}. \tag{4}$$

The DFT output is passed through maximal ratio combining (MRC). The $\ell'^{\,th}$ bit of the combiner output is obtained as follows:

$$b^{u}(\ell') = \sum_{n'=0}^{N-1} Z_{\ell',n'} g_{\ell',n'} C^{u}(n'). \tag{5}$$

For MRC, the combiner gain is given as:

$$g_{\ell',n'} = H^{*}_{\ell',n'}, \tag{6}$$

where $H_{\ell',n'}$ is the envelope of the $(\ell',n')^{\text{th}}$ subcarrier and $H^{*}_{\ell',n'}$ is the complex conjugate of $H_{\ell',n'}$.

For $n' = n$, $i = 0$, and $u = 0$, the right-hand side of Eq. (5) can be decomposed into parts due to useful power, ISI, intercarrier interference (ICI), multiple access interference (MAI), and AWGN, or b_U, b_{ISI}, b_{ICI}, b_{MAI}, and b_{AWGN}, respectively.

$$\begin{aligned} b^{0}_{U}(\ell' = \ell) = \sqrt{\tfrac{NL}{NL+\upsilon}E_s} \sum_{k=0}^{NL-1} \tfrac{1}{NL} \sum_{\phi=-\upsilon}^{NL-1} \sum_{n=0}^{N-1} a^{0}_{0}(\ell)\, C^{o}(n)\; h(k-\phi)\; g_{\ell,n}\, C^{o}(n) \\ \times\; e^{j2\pi\phi\frac{(N\ell+n)}{NL}} e^{-j2\pi k\frac{(N\ell+n)}{NL}} \end{aligned} \tag{7}$$

$$\begin{aligned} b^{0}_{ICI}(\ell') = \sqrt{\tfrac{NL}{NL+\upsilon}E_s} \sum_{k=0}^{NL-1} \tfrac{1}{NL} \sum_{\phi=-\upsilon}^{NL-1} \sum_{n=0}^{N-1} a^{0}_{0}(\ell') C^{o}(n)\, h(k-\phi)\; g_{\ell',n}\, C^{o}(n) \\ \times\; e^{j2\pi\phi\frac{(N\ell+n)}{NL}} e^{-j2\pi k\frac{(N\ell'+n)}{NL}} \end{aligned} \tag{8}$$

$$\begin{aligned} b^{0}_{ISI}(i,\ell') = \sqrt{\tfrac{NL}{NL+\upsilon}E_s} \sum_{k=0}^{NL-1} \tfrac{1}{NL} \sum_{\phi=-\upsilon}^{NL-1} \sum_{n=0}^{N-1} a^{0}_{i}(\ell') C^{o}(n)\; h\left[(k-\phi) - i\left(NL+\upsilon\right)\right] \\ \times\; g_{\ell',n} C^{o}(n)\; e^{j2\pi\phi\frac{(N\ell+n)}{NL}} e^{-j2\pi k\frac{(N\ell'+n)}{NL}} \end{aligned} \tag{9}$$

$$b^0_{MAI}(u,i,\ell') = \sqrt{\frac{NL}{NL+\upsilon}E_s}\sum_{k=0}^{NL-1}\frac{1}{NL}\sum_{\phi=-\upsilon}^{NL-1}\sum_{n=0}^{N-1}a^u_i(\ell')C^u(n)\;h\left[(k-\phi)-i\left(NL+\upsilon\right)\right] \times\; g_{\ell',n}\,C^o(n)\;e^{j2\pi\phi\frac{(N\ell+n)}{NL}}e^{-j2\pi k\frac{(N\ell'+n)}{NL}} \tag{10}$$

$$b^0_{AWGN} = \sqrt{\frac{1}{NL}}\sum_{k=0}^{NL-1}\sum_{n=0}^{N-1}g_{\ell',n}\,C^o(n)\,w\left(k\right)e^{-j2\pi k\frac{(N\ell'+n)}{NL}} \tag{11}$$

Using the parts b_U, b_{ISI} b_{ICI}, b_{MAI}, and b_{AWGN} from Eqs. (7)-(11), the powers P_U, P_{ISI}, P_{ICI}, P_{MAI}, and P_{AWGN} can be expressed as shown below.

$$P_U = E\left\{\left|b^{(}_U\ell'=\ell)\right|^2\right\} \tag{12}$$

$$P_{ICI} = \sum_{\substack{\ell'=0\\ \ell'\neq\ell}}^{L-1} E\left\{\left|b^{(}_{ICI}\ell')\right|^2\right\} \tag{13}$$

$$P_{ISI} = \sum_{\substack{i=-\infty\\ i\neq 0}}^{+\infty}\sum_{\ell'=0}^{L-1}E\left\{\left|b^{(}_{ISI}i,\ell')\right|^2\right\} \tag{14}$$

$$P_{MAI} = \sum_{u=1}^{U-1}\sum_{i=-\infty}^{+\infty}\sum_{\ell'=0}^{L-1}E\left\{\left|b^0_{MAI}(u,i,\ell')\right|^2\right\} \tag{15}$$

$$P_{AWGN} = E\left\{\left|b^0_{AWGN}\right|^2\right\} \tag{16}$$

Here, $E\{\cdot\}$denotes expectation.

2.3. Mobile radio channel

Measurement-based channel models were used in this study. The propagation measurements were previously carried out in the center of Manchester, England, within the 2110-2170 MHz band using a chirp sounder. Details of the sounder and the measurements can be found in [17]. In brief, the channel was sampled using repetitive chirp-based signals at numerous locations, and the sounding technique allowed the channel impulse response for a band of interest within the swept band to be obtained by choosing the corresponding subsection of the data. The power delay profile (PDP) was then calculated as the ensemble average of a number of impulse responses of the channel measured over a small-scale time interval or spatial displacement.

In a mobile radio channel, the received signal will be spread over time. The time dispersive properties of multipath channels are widely characterized by their average delay, rms delay spread, and delay window [18,19]. The average delay is the first moment of the PDP. The rms delay spread is the square root of the second central moment of the PDP. The delay window (W_q) is the duration of the middle portion of the PDP that contains q% of the total multipath power (Figure 2). The total multipath power ($\mathrm{P}_{m,tot}$) is the sum of multipath power above the noise threshold. Here we will refer to W_q as the q% delay window. The boundaries of the delay

window are determined in such a way that the power outside the window is split into 2 equal parts [18]. The $q\%$ delay window is given by:

$$W_q = \tau_2 - \tau_1, \tag{17}$$

$$\int_{\tau_1}^{\tau_2} P_h(\tau)\, d\tau = \frac{q}{100} \int_{\tau_0}^{\tau_3} P_h(\tau)\, d\tau = \frac{q}{100}\, P_{m,tot}, \tag{18}$$

where τ_1 and τ_2 denote the boundaries of the delay window. For the parts outside the delay window, we can write:

$$\int_{\tau_0}^{\tau_1} P_h(\tau)\, d\tau = \int_{\tau_2}^{\tau_3} P_h(\tau)\, d\tau = \frac{(1-q/100)}{2} \int_{\tau_0}^{\tau_3} P_h(\tau)\, d\tau = \frac{(1-q/100)}{2}\, P_{m,tot}, \tag{19}$$

where τ_0 and τ_3 are the end points of the PDP above the noise threshold and $\mathrm{P}_h(\tau)$ is the PDP of the channel, i.e. $P_h(\tau) = E\left\{|h(\tau)|^2\right\}$ where $E\{\cdot\}$ denotes the expectation operator.

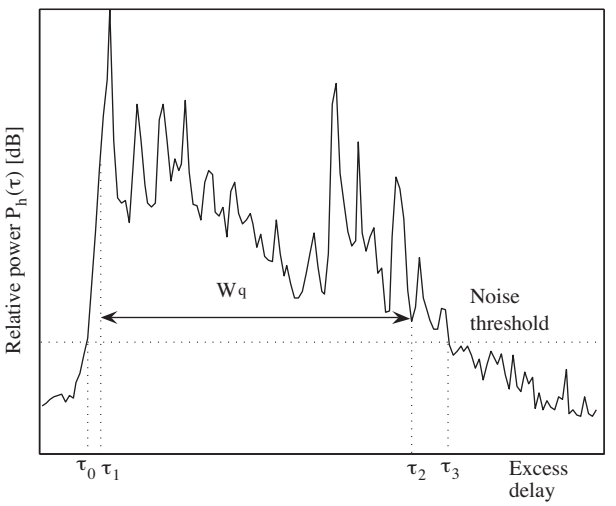

Figure 2. A PDP illustrating q% delay window W_q.

Channel data from 23 outdoor locations for the middle 40-MHz section of the 2110-2170 MHz band were used for analysis in this study. For each channel, impulse response estimates for every 4 ms were obtained, with the channel being assumed stationary within each 4 ms. Three of these estimates, referred to as channels 1, 2, and 3 (Ch1, Ch2, and Ch3) were selected for detailed illustrations. The maximum Doppler shifts observed were 40 Hz, 27 Hz, and 30 Hz for Ch1, Ch2, and Ch3, respectively. Figure 3 illustrates the PDPs for the 3 channels. The value of the rms delay spread was 0.22 μs for Ch1, 0.77 μs for Ch2, and 1.14 μs for Ch3. Based on the statistics presented in [17], Ch1, Ch2, and Ch3 are representative of small, mild, and strong multipath spreads for outdoor radio channels, respectively. For Ch1, the first arriving multipath component contains about 90% of the total multipath energy. For Ch3, the strongest component (by at least 10 dB above all others) was at the excess delay of 3.1 μs. For Ch2 and Ch3, the PDPs are nonexponentially decaying.

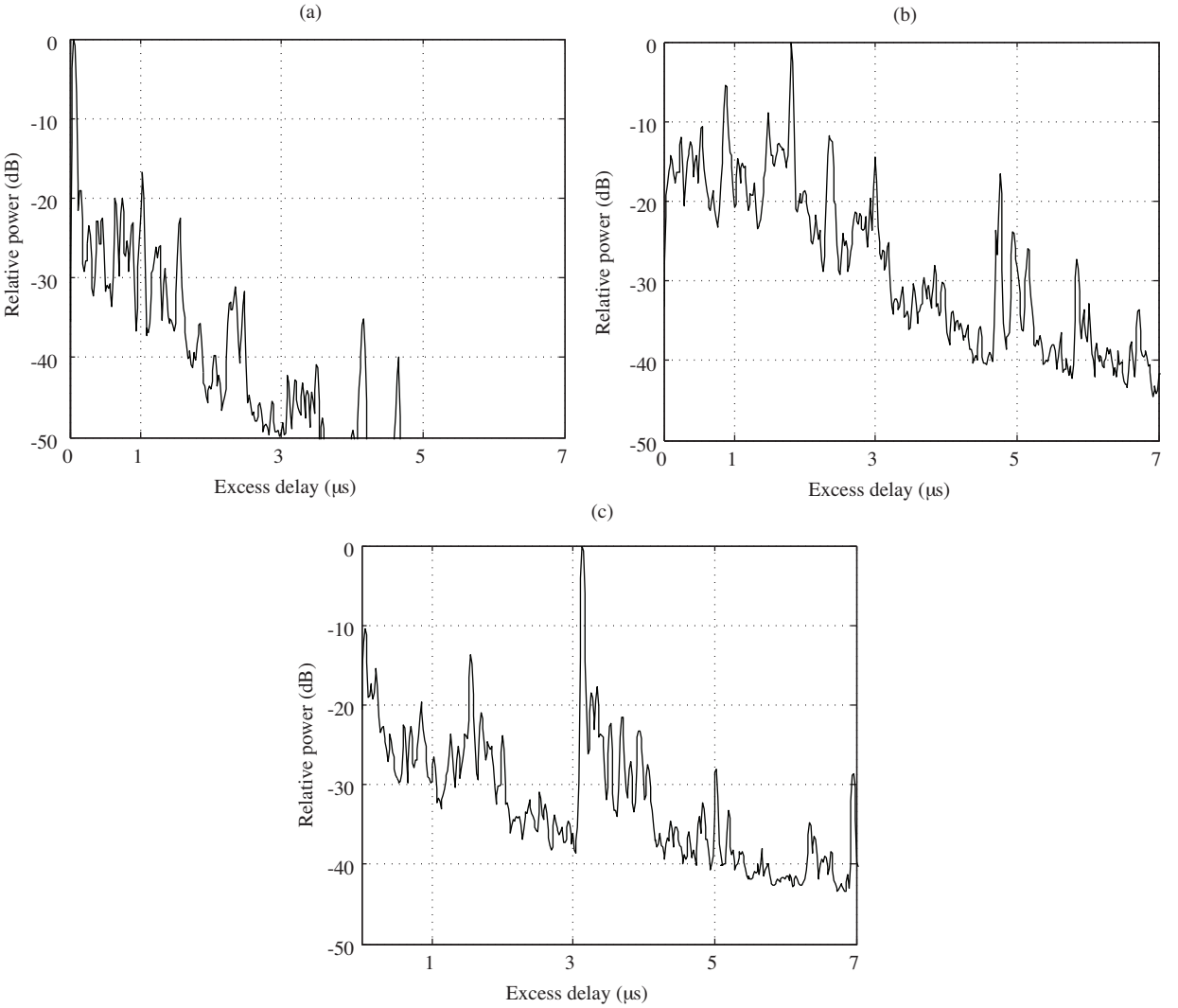

Figure 3. Power delay profiles for a) Ch1, b) Ch2, and c) Ch3.

3. The effect of the guard interval on system performance

In this work, the system performance is determined from the SNR level of a detected bit by considering the power present within the guard interval and the ISI caused by insufficient guard interval, ICI, and the presence of AWGN.

In MC-CDMA systems, the power for the ℓ^{th} bit after the combining can be given as:

$$P(\ell) = E_s \left(\frac{NL}{NL+v} \right) \left[P_U(\ell) + P_{ISI}(\ell) + P_{ICI}(\ell) + P_{MAI}(\ell) \right] + N_0, \tag{20}$$

where P_U is the useful power, P_{ISI} is the ISI power, P_{ICI} is the ICI power, P_{MAI} is the MAI power, and N_0 is the AWGN power. The factor $\left(\frac{NL}{NL+v} \right)$ is included in the expression to account for power loss within the guard interval. As the durations of $NL + v$ and NL chips correspond to the symbol period and the interval

(T_s-T_G), respectively, the above equation can be rewritten as follows:

$$P(\ell) = E_s\left(1 - \frac{T_G}{T_s}\right)\left[P_U(\ell) + P_{ISI}(\ell) + P_{ICI}(\ell) + P_{MAI}(\ell)\right] + N_0. \tag{21}$$

The SNR for the ℓ^{th} bit is the ratio of the useful power to the noise/interference powers; it can be written as:

$$\left(\frac{S}{N}\right)_\ell = \frac{E_s\left(1 - \frac{T_G}{T_s}\right)P_U(\ell)}{E_s\left(1 - \frac{T_G}{T_s}\right)\left[P_{ISI}(\ell) + P_{ICI}(\ell) + P_{MAI}(\ell)\right] + N_0}. \tag{22}$$

This equation can be rewritten as:

$$\left(\frac{S}{N}\right)_\ell = \frac{E_s}{N_0}\cdot\left[\frac{\left(1 - \frac{T_G}{T_s}\right)P_U(\ell)}{1 + \frac{E_s}{N_0}\left(1 - \frac{T_G}{T_s}\right)\left(P_{ISI}(\ell) + P_{ICI}(\ell) + P_{MAI}(\ell)\right)}\right]. \tag{23}$$

The second (bracketed) term on the right-hand side of the equation is referred to as the guard factor (GF) in this work. The GF depends on T_G, T_S, E_s/N_0, the channel profile, and separate powers P_U, P_{ISI}, and P_{ICI}. The GF can be used to determine the deterioration of the performance with respect to these parameters.

The guard interval is optimized for a single user system as in [10]. For this case, $P_{MAI} = 0$ and the GF (for the ℓ^{th} bit) in dB can be written as:

$$GF = 10\log\left(\frac{\left(1 - \frac{T_G}{T_s}\right)P_U(\ell)}{1 + \frac{E_s}{N_0}\left(1 - \frac{T_G}{T_s}\right)\left[P_{ISI}(\ell) + P_{ICI}(\ell)\right]}\right). \tag{24}$$

For this performance measure, it is necessary to determine powers P_U, P_{ISI}, and P_{ICI}. These powers depend on T_G and the channel PDP.

4. Numerical results

The MC-CDMA system parameters used in the analysis are listed in Table 1. Analysis was carried out for a 40-MHz transmission bandwidth. The spreading code used was a Walsh-Hadamard orthogonal variable spreading factor (OVSF) code with a spreading factor of 4. Increasing the number of subcarriers beyond 256 for Ch1, 1024 for Ch2, and 2048 for Ch3 had a negligible effect on performance [20,21], and these were therefore selected. We chose 2 representative values of E_s/N_0 to determine the optimum guard interval. A value of 10 dB represents the point at which the performances of different techniques start to diverge [5,10,14]. A value of 20 dB represents a typical high SNR value. Channel profiles were normalized so that total multipath energy in each case was equal to unity. For each channel normalized, the $P_{U,norm}$, $P_{ISI,norm}$, and $P_{ICI,norm}$ powers were determined, and from these, GFs for varying lengths of the guard interval were calculated. The optimum guard interval was determined to be the guard interval that resulted in the maximum GF. Finally, the relationship of the optimum guard interval to τ_{rms}, T_s, and W_q was investigated.

Table 1. System parameters and channel properties.

Number of users	Single user		
Uplink/downlink	Downlink		
Spreading code	Walsh-Hadamard OVSF		
Code length, N	4		
(Gain) combining	MRC		
Transmission bandwidth, B	40 MHz		
Channel model	Ch1	Ch2	Ch3
Number of subcarriers	256	1024	2048
τ_{rms}	0.22 μs	0.77 μs	1.14 μs
Symbol period, T_s	6.4 μs	25.6 μs	51.2 μs

4.1. Optimum guard interval

For each of the 3 channel models, the effect of guard interval on normalized useful power ($P_{U,norm}$) is illustrated in Figure 4. For a clearer illustration, values of $P_{U,norm}$ were restricted in the range of 0.98 to 1.

In Figure 4, we observe that the value of $P_{U,norm}$ increases with increasing guard interval and approaches unity at about 2.5 μs, 6.25 μs, and 7.5 μs for Ch1, Ch2, and Ch3, respectively. Figure 4 can also provide information on interference power, as the sum of useful and interference powers in a normalized PDP is equal to unity, or $P_{ISI,norm} + P_{ICI,norm} = 1 - P_{U,norm}$. In the case of normalized powers, the guard factor is unity for $T_G = 0$ and interference-free communication.

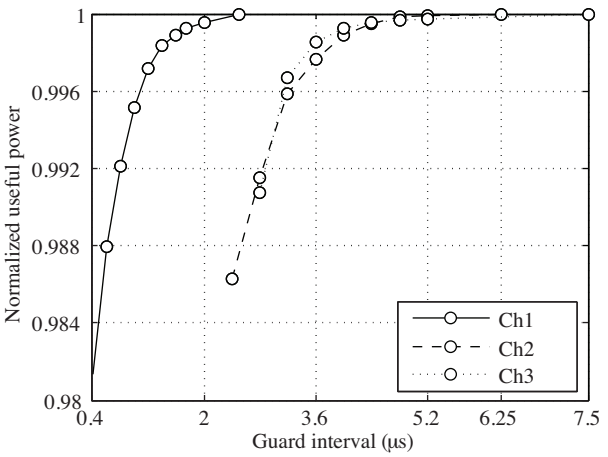

Figure 4. $P_{U,norm}$ values for Ch1, Ch2, and Ch3.

Figure 5 shows the effect of AWGN and the guard interval for the 3 channels using Eqs. (12)-(14), (16), and (24) for $E_s/N_0 = 10$ dB and $E_s/N_0 = 20$ dB. The optimum guard interval is affected by E_s/N_0. The optimum guard interval for Ch1 was 0.6 μs for $E_s/N_0 = 10$ dB and 1.4 μs for $E_s/N_0 = 20$ dB (Figure 5a); for Ch2, these were 2.8 μs and 4.8 μs, respectively (Figure 5b); and for Ch3, these were 3.6 μs and 4.8 μs (Figure 5c).

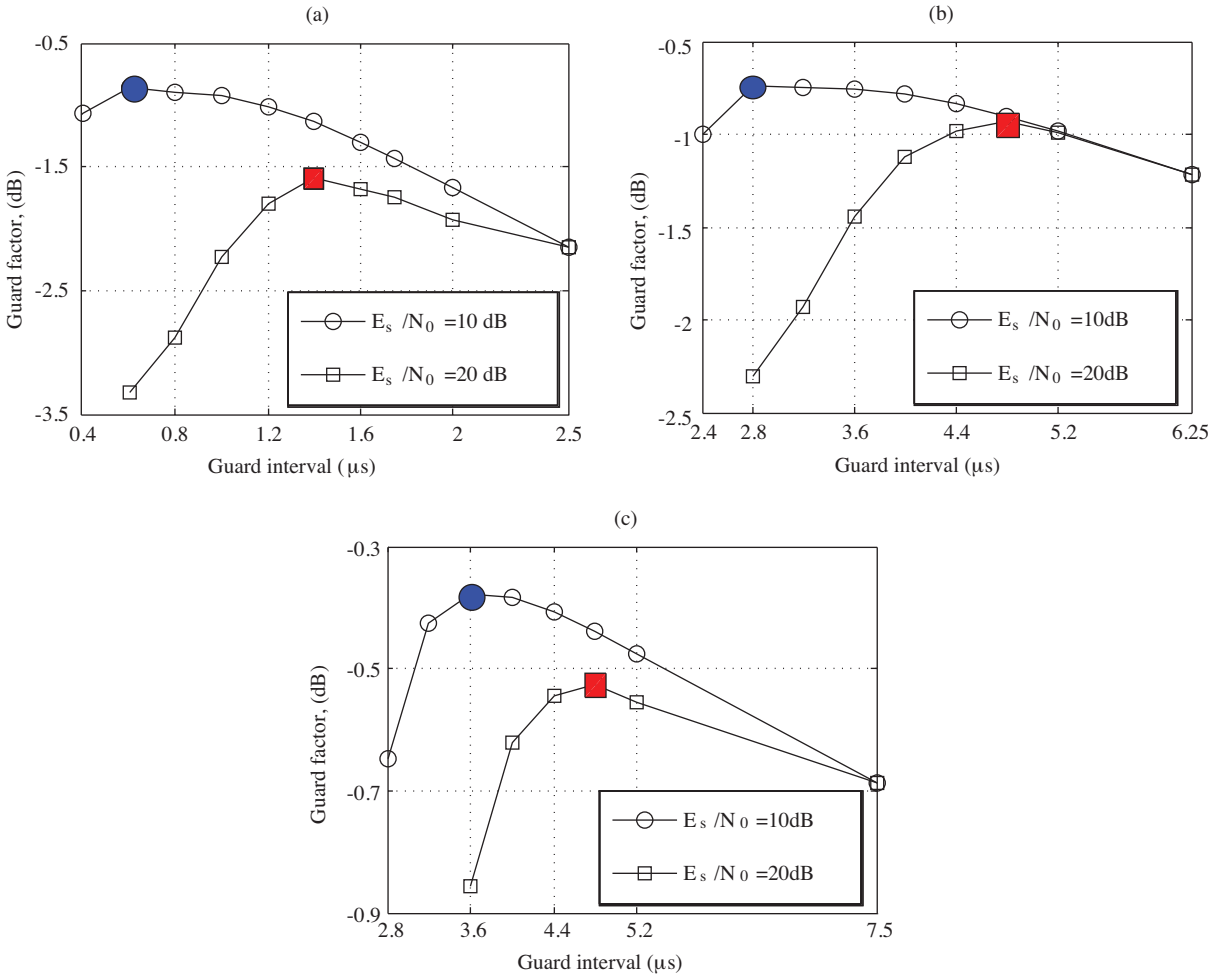

Figure 5. Guard factors for $E_s/N_0 = 10$ dB and $E_s/N_0 = 20$ dB for a) Ch1, b) Ch2, and c) Ch3.

For guard intervals shorter than the optimum ($T_G < T_{G,opt}$), the performance deterioration is due to the ISI caused by the part of the impulse response exceeding the guard interval. For $T_G > T_{G,opt}$, the deterioration is due to the power loss within the guard interval. It can be observed that with an increasing guard interval, the curves of the GF become less dependent on the value of E_s/N_0. This would be expected from Eq. (24), as the interference power becomes negligible as $P_{U,norm}$ approaches unity.

4.2. Optimum guard interval and rms delay spread

Table 2 lists the optimum guard interval, its ratio to τ_{rms}, the ratio of the symbol period to $T_{G,opt}$, and $q\%$ values for $W_q = T_{G,opt}$ for the 3 channels. The optimum guard interval varied between 2.7 τ_{rms} and 3.6 τ_{rms} for $E_s/N_0 = 10$ dB and between 4.2 τ_{rms} and 6.4 τ_{rms} for $E_s/N_0 = 20$ dB.

To better characterize the relationship between $T_{G,opt}$ and τ_{rms}, mobile radio channel data from 20 further small-scale locations [17] were used for analysis. The scatter plot of optimum guard interval versus rms delay spread, in Figure 6, shows that the optimum guard interval varied between 2 τ_{rms} and 4 τ_{rms} for $E_s/N_0 = 10$ dB (Figure 6a) and between 3 τ_{rms} and 6.4 τ_{rms} for $E_s/N_0 = 20$ dB (Figure 6b), with points mainly scattered around the line $T_{G,opt} = 3\tau_{rms}$ for $E_s/N_0 = 10$ dB and $T_{G,opt} = 4\tau_{rms}$ for $E_s/N_0 = 20$ dB. The

cross-correlation between the optimum guard interval and the rms delay spread was 0.91 with a 95% confidence interval of 0.79 and 0.96 for $E_s/N_0 = 10$ dB. For $E_s/N_0 = 20$ dB, it was 0.917 with a confidence interval of 0.80 and 0.967. Regression analysis of the 2 parameters gave $T_{G,opt} \cong 2.83\tau_{rms}$ for $E_s/N_0 = 10$ dB and $T_{G,opt} \cong 3.92\tau_{rms}$ for $E_s/N_0 = 20$ dB.

Table 2. Values of $T_{G,opt}$, their relation to τ_{rms} and T_s, and percentages of multipath energy contained within $T_{G,opt}$ for Ch1, Ch2, and Ch3.

Channel	$E_s/N_0 = 10$ dB				$E_s/N_0 = 20$ dB			
	$T_{G,opt}$ (μs)	$\frac{T_{G,opt}}{\tau_{rms}}$	$\frac{T_s}{T_{G,opt}}$	$q\%$	$T_{G,opt}$ (μs)	$\frac{T_{G,opt}}{\tau_{rms}}$	$\frac{T_s}{T_{G,opt}}$	$q\%$
Ch1	0.6	2.7	10.7	93	1.4	6.4	4.6	99
Ch2	2.8	3.6	9.1	95	4.8	6.2	5.3	99
Ch3	3.6	3.1	14.2	96	4.8	4.2	10.7	99

Further analysis revealed that PDPs with an exponentially decaying profile required a guard interval that was greater than 5 times the rms delay spread (5 τ_{rms}) for $E_s/N_0 = 20$ dB. Those having either only a few strong components or a late-arriving cluster with strong components required a guard interval between 3 τ_{rms} and 4 τ_{rms}. Although we employed the MRC gain combining technique, which is known to have a poor ability to combat ISI and may therefore require longer guard intervals, our results compare well with those for minimum mean-square error (MMSE) combining techniques. For example, [11] also found that the guard interval for MMSE should be at least 4 times the rms delay spread for an exponentially decaying PDP.

Our data contain further types of profiles not previously considered in the literature and not matching traditional models. These data result not only in a different value of the $T_{G,opt}/\tau_{rms}$ ratio, but a value that can be dependent on E_s/N_0. For example, if components arrive as an initial cluster, with a few strong components followed by a much later cluster of slow-decaying components largely below –20 dB, this will result in $T_{G,opt}/\tau_{rms} \cong 2$ for $E_s/N_0 = 10$ dB, but $T_{G,opt}/\tau_{rms} \cong 6$ for $E_s/N_0 = 20$ dB.

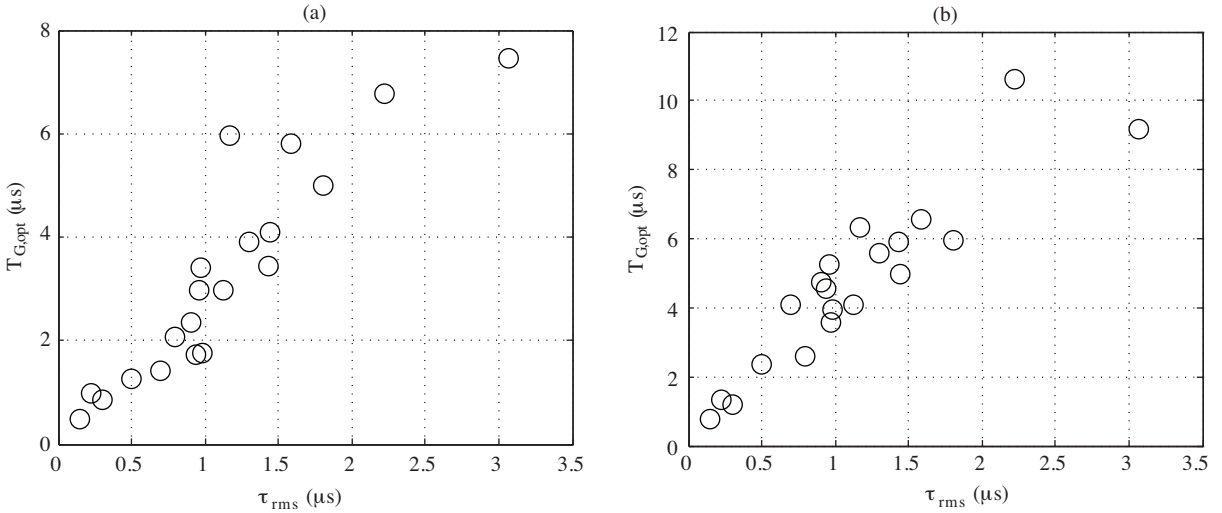

Figure 6. $T_{G,opt}$ versus τ_{rms} for 20 measured channel models for a) $E_s/N_0 = 10$ dB and b) $E_s/N_0 = 20$ dB.

4.3. Optimum guard interval and delay window

We investigated whether there was a relationship between our value for the optimum guard interval and the percentage multipath energy, q%, held within the corresponding delay window (i.e. $W_q = T_{G,opt}$). Such a rule would predict the optimum guard interval for a given channel PDP without the need for a computationally complex GF calculation.

The percentages of the multipath energy held within the delay window for $W_q = T_{G,opt}$ are given in Table 2. In this case, for $E_s/N_0 = 10$ dB, the optimum guard interval gave delay windows for the 3 channels that contained multipath power that ranged from 93% to 96%, and this might be generalized to be around 95%. For example, Ch1 had delay windows of 0.6 μs and 1.4 μs containing 93% and 99% of the multipath energy, respectively. For $E_s/N_0 = 20$ dB, the optimum guard interval gave a delay window that contained about 99% of the multipath power.

The rule for the optimum guard interval and delay window was validated by testing the remaining 20 small-scale locations. As a test for each location, we determined the values of the optimum guard intervals and the delay windows with 92%, 95%, 96%, 97%, 98%, 99%, and 100% of multipath power. The values of the 92%, 95%, 96%, and 97% delay windows are shown in a scatter plot in Figure 7a against the corresponding optimum guard interval for $E_s/N_0 = 10$ dB. The solid lines indicate $W_q = T_{G,opt}$. The values of the 98%, 99%, and 100% delay windows are shown in a scatter plot in Figure 7b against the corresponding optimum guard interval for $E_s/N_0 = 20$ dB. In general, almost all of the values lying on the line $W_q = T_{G,opt}$ correspond to W_{95} in the case of $E_s/N_0 = 10$ dB and to W_{99} in the case of $E_s/N_0 = 20$ dB. We included the 100% delay windows in Figure 7b to demonstrate the significant difference between the 99% and 100% delay windows.

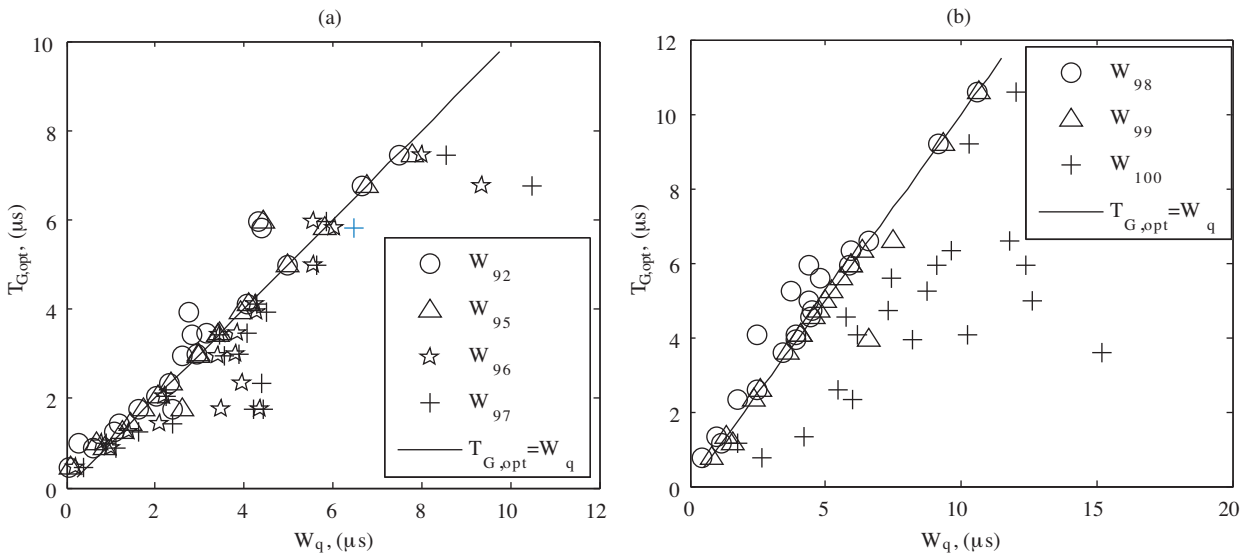

Figure 7. $T_{G,opt}$ versus delay windows a) for $E_s/N_0 = 10$ dB and b) for $E_s/N_0 = 20$ dB.

In order to investigate the relationship between the optimum guard interval and the delay window, we determined their cross-correlation factors. For $E_s/N_0 = 10$ dB, the cross-correlation between the optimum guard interval and a 95% delay window was found to be 0.979 with a 95% confidence interval between 0.95 and 0.99. For $E_s/N_0 = 20$ dB, the correlation between the optimum guard interval and a 99% delay window was found to be 0.97 with a confidence interval between 0.93 and 0.99. These correlation values are higher than

those between the optimum guard interval and the rms delay spread, and they indicate that a 95% or 99% delay window better represents the optimum guard intervals for $E_s/N_0 = 10$ dB and $E_s/N_0 = 20$ dB, respectively.

Based on our results, we propose the empirical rule that the guard interval may be set to the delay window containing 95% and 99% of multipath power for $E_s/N_0 = 10$ dB and $E_s/N_0 = 20$ dB, respectively, if it is to avoid ISI and be optimum in the sense of maximizing the SNR.

This compares with the 2-ray equal-power profile, where the ratio of $T_{G,opt}/\tau_{rms}$ must take on a value slightly greater than 2 if it is to hold more than 90% of the multipath energy, so that it accommodates the second arriving component that has an excess delay of 2 τ_{rms}. In this case, it will hold 100% of the multipath energy. Our results for $T_{G,opt}$ versus τ_{rms} (Section 3.3) all had an optimum guard interval that was greater than 2 τ_{rms} for both $E_s/N_0 = 10$ dB and $E_s/N_0 = 20$ dB, and we conclude that none of our data had a 2-ray equal-power profile. Although the 2-ray equal-power profile can be used in the optimization of the number of subcarriers, it is not suitable for the optimization of the guard interval.

5. Conclusion

In this paper, an analytical expression for calculating SNR was derived and used as a measure of performance to determine the optimum guard interval for MC-CDMA systems. The guard interval giving the maximum SNR was determined to be the optimum guard interval $T_{G,opt}$.

The results showed that the optimum guard interval varied between 2 τ_{rms} and 4 τ_{rms} for $E_s/N_0 = 10$ dB and between 3 τ_{rms} and 6.4 τ_{rms} for $E_s/N_0 = 20$ dB. The characteristics of the PDPs affected $T_{G,opt}$ as well as the rms delay spread value. For a high SNR per symbol, such as 20 dB of E_s/N_0, exponentially decaying profiles were found to have worst-case guard intervals.

An empirical rule based on actual data was derived for the optimum guard interval and delay window for $E_s/N_0 = 10$ dB and $E_s/N_0 = 20$ dB. The delay windows with approximately 95% and 99% of multipath energy were found to be a good choice for guard intervals for $E_s/N_0 = 10$ dB and $E_s/N_0 = 20$ dB.

References

[1] R. Prasad, R.S. Hara, "Overview of multicarrier CDMA", IEEE Communications Magazine, pp. 126-133, 1997.

[2] N. Yee, J.P. Linnartz, G. Fettweis, "Multi-carrier CDMA in indoor wireless radio networks", Proceedings of IEEE Personal Indoor and Mobile Radio Communications, pp. 468-472, 1993.

[3] K. Fazel, S. Kaiser, Multi-Carrier and Spread Spectrum Systems, Chichester, John Wiley & Sons, 2003.

[4] K. Adachi, F. Adachi, M. Nakagawa, "Cellular MIMO channel capacities of MC-CDMA and OFDM", IEEE Vehicular Technology Conference, pp. 1980-1984, 2008.

[5] A.S. Ling, L.B. Milstein, "The effect of spatial diversity and imperfect channel estimation on wideband MC-DS-CDMA and MC-CDMA", IEEE Transactions on Communications, Vol. 57, pp. 2987-3000, 2009.

[6] R.V. Nee, R. Prasad, OFDM for Wireless Multimedia Communications, Boston, Artech House, 2000.

[7] P. Torres, A. Gusmao, "Iterative receiver technique for reduced-CP, reduced-PMEPR OFDM transmission", IEEE Vehicular Technology Conference, pp. 1981-1985, 2007.

[8] B.M. Masini, F. Zabini, "On the effect of combined equalization for MC-CDMA systems in correlated fading channels", IEEE Wireless Communications and Networking Conference, pp. 1-6, 2009.

[9] A.B. Djebbar, K. Abed-Meraim, A. Djebbari, "Blind and semi-blind equalization of downlink MC-CDMA system exploiting guard interval redundancy and excess codes", IEEE Transactions on Communication, Vol. 51, pp. 156-163, 2009.

[10] S. Hara, R. Prasad, "Design and performance of multicarrier CDMA system in frequency-selective Rayleigh fading channels", IEEE Transactions on Vehicular Technology, Vol. 48, pp. 1584-1595, 1999.

[11] E. Kunnari, J. Iinatti, "Performance analysis of multirate MC-CDMA in Rayleigh-fading channels with delay power spectrum exceeding the guard interval", IEEE Journal on Selected Areas in Communications, Vol. 24, pp. 542-543, 2006.

[12] M.J. Gans, "A power-spectral theory of propagation in the mobile radio environment", IEEE Transactions on Vehicular Technology, Vol. 21, pp. 27-38, 1972.

[13] B.H. Fleury, "An uncertainty relation for WSS process and its application to WSSUS systems", IEEE Transactions on Communications, Vol. 44, pp. 1632-1634, 1996.

[14] B.S. Lee, S.C. Park, "Design and performance analysis of the MC-CDMA", Proceedings of 14th IEEE International Symposium on Personal, Indoor and Mobile Radio Communication, Vol. 3, pp. 2230-2233, 2003.

[15] A.C. McCormick, E.A. Al-Susa, "Multicarrier CDMA for future generation mobile communication", Electronics & Communication Engineering Journal, Vol. 14, pp. 52-60, 2002.

[16] S. Le Nours, F. Nouvel, J.F. Helard, "Design and implementation of MC-CDMA systems for future wireless networks", EURASIP Journal on Applied Signal Processing, Vol. 2004, pp. 1604-1615, 2004.

[17] S. Salous, H. Gokalp, "Medium and large-scale characterization of UMTS allocated frequency-division duplex channels", IEEE Transactions on Vehicular Technology, Vol. 56, pp. 2831-2843, 2007.

[18] J.D. Parsons, The Mobile Radio Propagation Channel, Chichester, John Wiley & Sons, 1992.

[19] T.S. Rappaport, Wireless Communications: Principles and Practice, New Jersey, Prentice Hall, 1996.

[20] Ç. Kurnaz, H. Gökalp, "Investigating MC-CDMA system performance using measurement-based channel models", 14th European Wireless Conference, 2008.

[21] Ç. Kurnaz, Investigating the Effect of Mobile Channel Parameters on MC-CDMA System Performance Using Analytical Modeling and Computer Simulation, PhD dissertation, Ondokuz Mayıs University, Samsun, Turkey, 2009.